Sensors and Actuators B 241 (2017) 1145–1152

Sensors and Actuators B: Chemical

journal homepage: www.elsevier.com/locate/snb

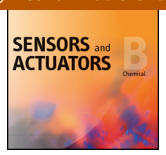

On the effects of the time gate position and width on the signal-to-noise ratio for detection of Raman spectrum in a time-gated CMOS single-photon avalanche diode based sensor

Ilkka Nissinen*, Jan Nissinen, Pekka Keränen, Juha Kostamovaara

Circuits and Systems Research Unit, University of Oulu, P.O. Box 4500, 90014, Finland

ARTICLE INFO

Article history:
Received 9 June 2016
Received in revised form 4 October 2016
Accepted 5 October 2016
Available online 8 October 2016

Keywords:
SPAD detector
Raman spectroscopy
Time gating
Single photon counting

ABSTRACT

The effects of the position and width of the time gate on the available signal-to-noise ratio in a time-gated Raman spectrometer are analyzed and measured. The Raman spectrometer used is based on a high power, 532 nm, pulsed laser (500 ps FWHM) and a time-resolving circuit with a single photon avalanche diode (SPAD) detector which is moved by a microstep motor to derive the whole Raman spectrum. The times of arrival of the scattered photons are recorded and the effectiveness of different time gate positions and widths are analyzed by post-processing the measured and simulated data. It is shown from measurements performed on olive and sesame seed oil samples having fluorescence lifetimes of 2.5 ns and 2 ns and Raman-to-fluorescence photon ratios of 0.03 and 0.003, respectively, that the fluorescence background can be substantially suppressed if the width and position of the time gate are properly selected.

1. Introduction

Raman spectroscopy is a well-known optical spectroscopic technique that gives information about the molecular structure and chemical environment of a sample. A CW (continuous wave) monochromatic laser operating in the visible, near-infrared or near-ultraviolet range is usually used as a light source for illuminating the sample [1,2]. A small number of incident photons interact with the vibrational states of the sample molecules and are then shifted from their original wavelength. For a certain vibrational or rotational mode of a specific molecule, the change in the energy of a Raman-scattered photon (the "Raman shift") is independent of the excitation photon energy. The Raman spectrum, i.e. the spectral distribution of the intensity of the Raman scattered photons, is unique for each chemical component and thus provides selectivity.

In addition, Raman spectroscopy gives well resolved spectral lines, and since it has a low sensitivity to water, it is also applicable to the study of biological and biochemical samples, which typically have a high water content [3]. It has therefore been used widely for substance identification and quantification in the agricultural, food, oil, pharmaceuticals and materials industries and for security control and crime investigations, for example [4–8].

Unfortunately, the measured Raman spectrum is masked by a strong fluorescence background in many of the potential applications. The reason for this is that the probability of Raman (cross-sectional) scattering is much lower than that of fluorescence [1,2,9]. In other words, Raman scattering and fluorescence emission are two competing phenomena and the spectrum is dominated by the most likely phenomenon, which is typically fluorescence, and thus it will induce a continuous background to the residual spectrum and especially increase the photon shot noise degrading the signal-to-noise ratio resulting in uncertainty in the case of both material identification and concentration measurements.

Fortunately, Raman and fluorescence scattered photons have different lifetimes. Raman photons are observed instantly during excitation, whereas fluorescence photons can still be detected after nanoseconds or even milliseconds, and thus the fluorescence background can be suppressed, if scattered photons are collected only during Raman scattering. This can be achieved by illuminating the sample with short, intensive laser pulses (pulse width much smaller than the fluorescence lifetime) rather than the traditional CW radiation and recording the sample response only during these short pulses, as depicted in Fig. 1 [9–12]. Thus, by "time-gating" the measurement to the period of the laser pulse, the probability of detecting fluorescence photons can be reduced, since these are mostly emitted after the Raman scattered photons. Furthermore, the accuracy of the baseline of the Raman spectrum is improved,

* Corresponding author.
E-mail address: ilkka.nissinen@ee.oulu.fi (I. Nissinen).

http://dx.doi.org/10.1016/j.snb.2016.10.021

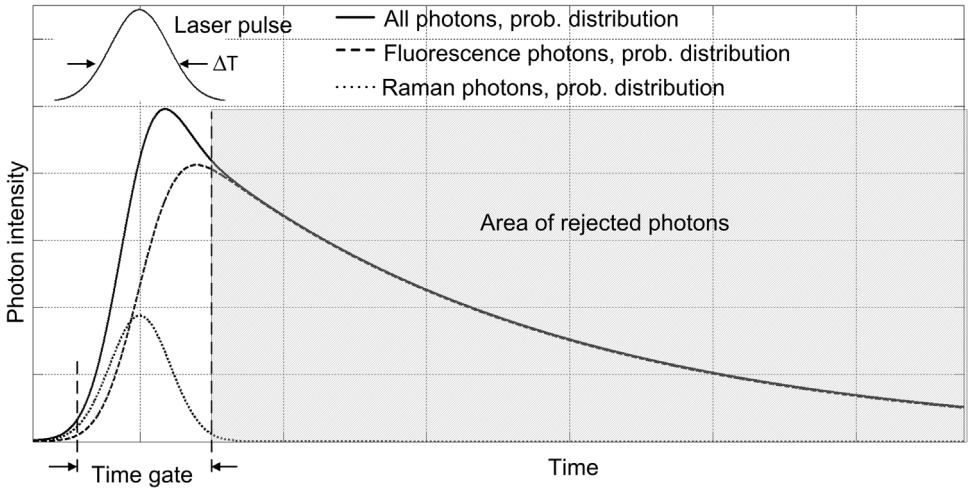

Fig. 1. Time gating principle.

which also leads to greater accuracy in both material identification and quantitative analysis.

Some earlier studies have implemented this "time-gating" technique by means of a high-speed optical shutter based on a Kerr cell [9] or a mode-locked laser with a spectrograph and intensified CCD (ICCD) [10]. In addition, some analysis has been done to ascertain the proper gate position of ICCD and CCD for achieving the best fluorescence rejection efficiency [11–14]. However, these devices are either highly sophisticated, physically large and expensive, or capable of measuring only a single wavelength band of the spectrum at a time, so that they require long measurement times and are thus unsuitable for on-site applications. To overcome these problems the CCDs and ICCD's should be replaced with more suitable detectors.

Single photon avalanche diodes (SPAD) having a single shot timing precision of 50.100 ps have been in use as optical detectors for some time. Various SPAD structures have been suggested by many groups, the aim having been to develop structures with adequate photon detection efficiency in standard CMOS technologies [15]. The use of a CMOS technology has also made it possible to design high-speed electronics together with SPADs on the same chip and has paved the way for the development of new detector chips for interesting applications, among them Raman spectroscopy. We have presented earlier a measurement set-up which uses a time-gated CMOS single photon avalanche detector (SPAD) to determine the time position of Raman-scattered photons with respect to the laser shot [16,17]. The use of a CMOS technology nevertheless allows us to fabricate 2-D SPAD array to derive the whole Raman spectrum, and some realizations have been presented with time gating resolutions from 100 ps to 1 ns [18–22]. A time gate of hundreds of picoseconds is adequate for many applications, but then the laser pulse width should be of the same value. A fluorescence rejection ratio of approximately 1:20, for example, can be achieved using a laser pulse width and time gate of 100 ps with a sample having a fluorescence time constant of 2 ns. The manufacture of a laser with a pulse width of less than 500 ps with high enough power and a narrow line width is a demanding task, however, so that it is hard to achieve the adequate fluorescence rejection ratio with the most demanding samples. As a consequence, when measuring a Raman spectrum for the most challenging samples a shorter laser pulse width together with a shorter, accurately positioned gate width or some other fluorescence suppression technique is needed.

We analyze here the effects of the position and width of the time gate in the case of challenging samples (with a high fluorescence background and short fluorescence lifetime) when using a moderate laser pulse width of 500 ps–1 ns. It is shown that by properly adjusting the width and position of the time gate, the signal-to-noise ratio of the Raman spectrum can be maximized. The technique is verified by measuring Raman spectra for olive oil and sesame seed oil samples with a "post-processed" time-gated Raman spectrometer based on a commercial pulsed laser having a wavelength and pulse width of 532 nm and 500 ps (FWHM), respectively, and a single photon avalanche diode detector with a 24 ps-resolution TAC. By using a single mechanically scanned detector, the ultimate achievable performance of the time-gated Raman spectroscopy device based on SPAD detectors can be estimated without the disturbing effect of the non-homogeneities of the widths and position of the time gate within a large SPAD detector array [19]. This gives valuable information for the development of large time-gated SPAD arrays from the point of view of the importance of the timing homogeneity of the width and time position of the time gates within the whole array. Sesame seed oil is known to be a difficult sample when used in Raman experiment at an excitation wavelength of 532 nm because of the very high fluorescence background and short time constant (~2 ns) [23].

In the following we first describe the structure of the time-gated Raman spectrometer, in Section 2, and then the fluorescence suppression technique, in Section 3. Section 4. gives some measurement results with demanding samples known to have a high fluorescence background, and the work is discussed and conclusions are drawn in Section 5.

2. Time-gated Raman spectroscopy using a CMOS SPAD with TDC and a pulsed laser

A block diagram of the time-gated Raman spectrometer environment used in this work is shown in Fig. 2. It consists of a 532 nm-pulsed laser (ΔT_{FWHM} = 500 ps, $\Delta\lambda$~0.1 nm) from Teem Photonic, a spectrograph based on a grating achieving approximately 10 cm^{-1} spectral resolution, a single passively-quenched SPAD, a time-to-amplitude converter (TAC) with a data analyzer (24 ps resolution), a microstep motor and an optical detector (DET) to synchronize the laser pulses with the output of the SPAD. Excitation is performed by a laser pulse having a pulse energy of 1.2 μJ and a spot size of ~100 μm at the surface of the sample with a pulse rate of 4 kHz. A small portion of the pulse is delivered to the optical detector to generate the start signal to the TAC. Photons from the sample are detected with a SPAD, which gives a stop signal to the TAC. The data analyzer collects the results from the TAC at each spectral point, i.e. each position of the step motor. Note that the

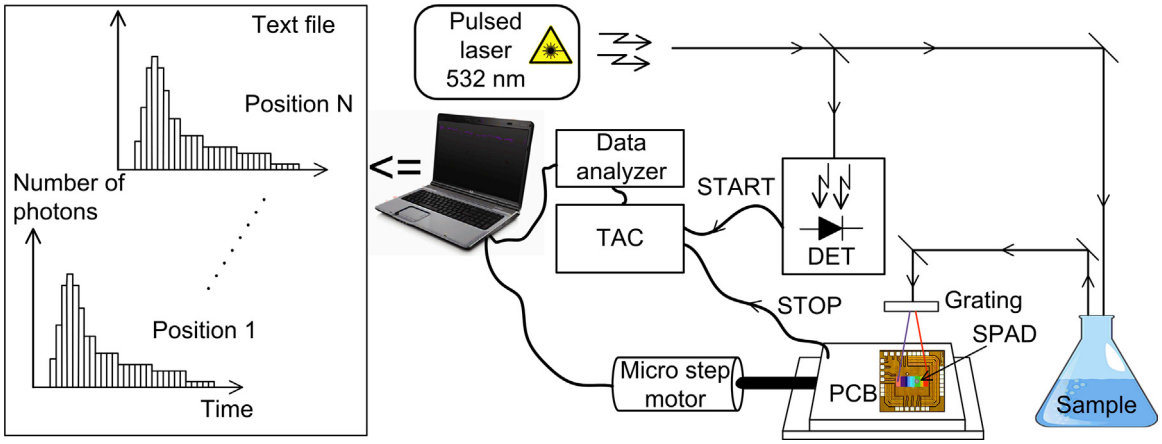

Fig. 2. Block diagram of the Raman setup.

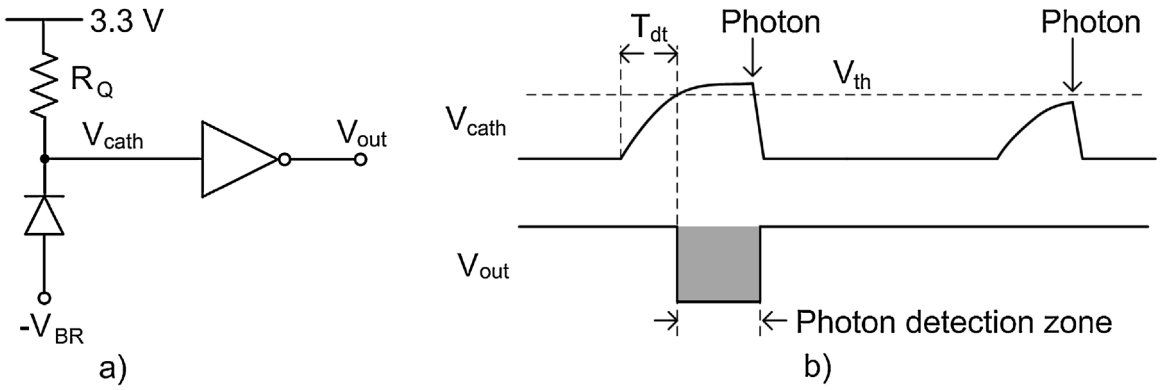

Fig. 3. a) Schematic and b) timing diagrams of the passively-quenched SPAD.

photon detection probability of the SPAD has to be much less than 1 within the desired measurement range so that the probability density function of photons from sample is not deteriorated by the pile-up in SPAD detector. The measurement is controlled with a programmable PC-card from National Instruments which sets the user-defined number of measurements at each spectral point, the start position and step size of the step motor and the number of steps. Histograms of the times of arrival of the photons (see Fig. 2 Text file) at each position (spectral point) are stored in the text file for later analysis. Thus post-processing fluorescence suppression can be performed by adjusting the time position and length of the time gate at a resolution of 24 ps as desired and the effectiveness of the suppression can be studied. In addition, residual fluorescence can be suppressed by using another time gate after the Raman signal to estimate the residual level at each spectral point and subtract this from the raw data [17].

Schematic and timing diagrams of a passively-quenched SPAD based on a structure presented previously [15,24] are shown in Fig. 3(a) and (b), respectively. The SPAD is a pn junction which is biased above the breakdown, i.e. in the Geiger mode, to detect single photons. The anode node has a negative high voltage equal to the breakdown voltage V_{BR} (~19 V) and the SPAD is biased above the breakdown through the resistor R_Q connected to a supply voltage of 3.3 V, giving an excess bias of approximately 3.3 V. The rise time of V_{cath} is determined by the quenching resistor and junction capacitance, resulting in a dead time of approximately100 ns (T_{dt} in Fig. 3(b)) when the threshold voltage of the inverter (V_{th} in Fig. 3(b)) is set close to the supply voltage, as shown in Fig. 3(b). As can be seen in Fig. 3(b), the second photon detected by the SPAD is not sensed by the inverter, because it occurs during its dead time. The measurements are not affected by the dead time, however, because this is much shorter than the time interval between the laser pulses (period of 250 μs). The buffered output (V_{out}) is connected to the stop channel of the TAC and its rising edge gives a stop timing signal to mark the detection of a photon.

3. Fluorescence suppression principle

The aim of this work was to study how the width and especially the position of the time gate should be chosen in order to achieve the best possible signal-to-noise ratio and thus the optimal fluorescence rejection ratio. To verify the analysis, Raman spectra were measured from olive and sesame seed oils having fluorescence time constants of approximately 2.5 ns and 2 ns, respectively [17].

Fig. 4(a) shows the Matlab-simulated Raman, fluorescence, dark count noise and combined photon probability distributions as functions of time when a Gaussian laser pulse (FWHM = 500 ps) is used for excitation. The ratio of the Raman to fluorescence photons, calculated as the ratio between the total numbers of these photons, is set to 0.3. The shape of the Raman photon distribution follows the excitation distribution, and the fluorescence distribution is derived as a convolution of the Gaussian function of the laser pulse and an exponentially decaying fluorescence lifetime function. The combined photon probability distributions are presented in Fig. 4(b) as a function of time with three different ratios of Raman to fluorescence photons. The number of Raman photons is kept constant and that of fluorescence photons is increased.

The effectiveness of the time gating can be evaluated in terms of the signal-to-noise ratio (SNR) with different time gate widths and

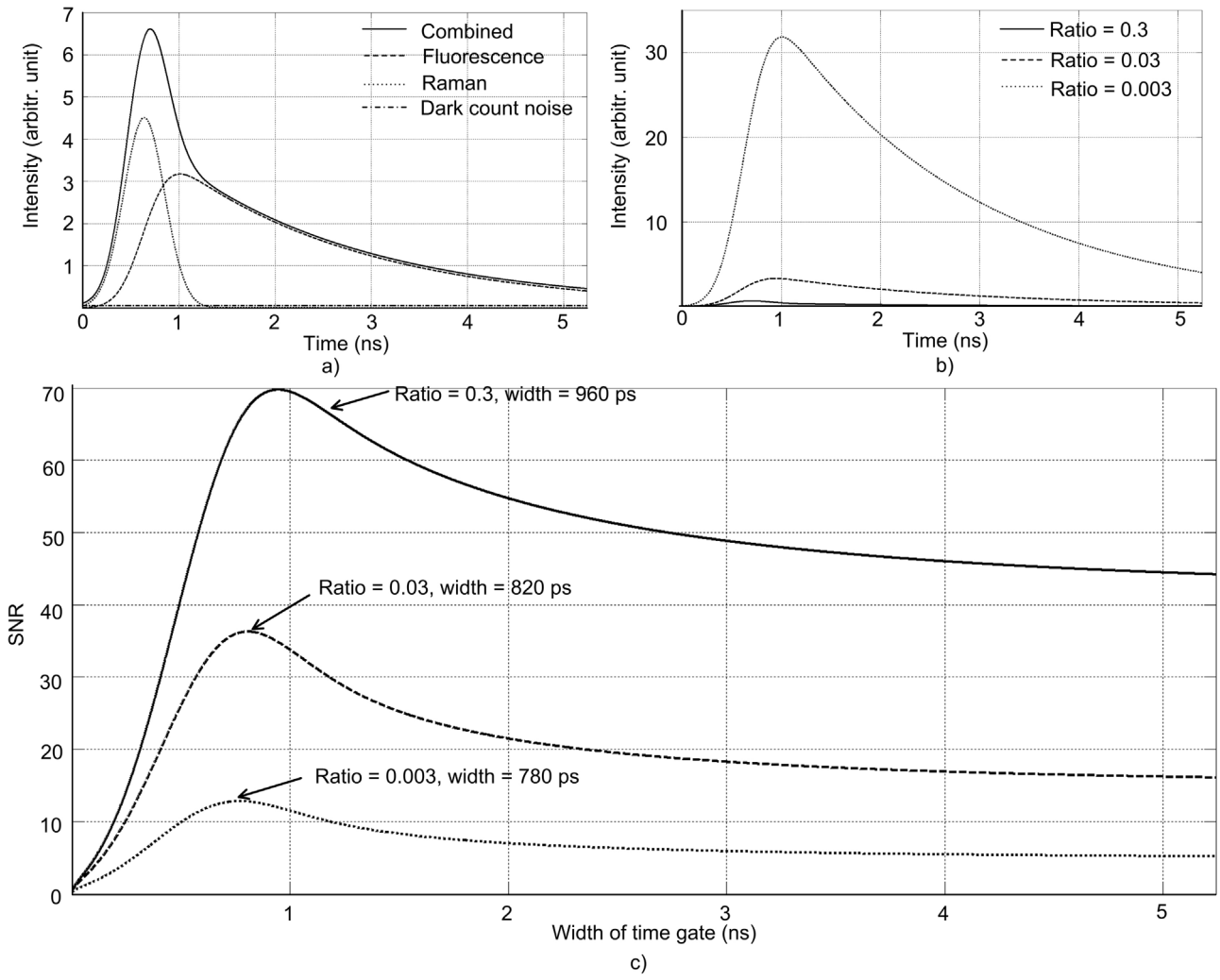

Fig. 4. a) Raman, fluorescence, dark count noise and combined photon probability density functions, b) combined probability density functions at different Raman to fluorescence ratios, and c) signal-to-noise ratios of 3,000,000 pulses as a function of the width of the time gate with Raman to fluorescence ratios 0.3, 0.03 and 0.003.

positions and different ratios of Raman to fluorescence photons. The SNR can be expressed as

$$SNR = \frac{N_R}{\sqrt{N_R + N_F + N_{DCR}}}, \quad (1)$$

where N_R, N_F and N_{DCR} are the numbers of detected Raman, fluorescence and dark count photons, respectively. As can be seen from Eq. (1), the shot noise is related to the numbers of Raman and fluorescence photons. Although fluorescence photons can be rejected by choosing the proper time gate width and position, some residual fluorescence will still be present within the time gate. The level of this residual fluorescence can be estimated by using another time gate to collect only the fluorescence photons after the Raman photons. This information can then be used for base line correction [17]. It should be noted, however, that this does not improve the signal-to-noise ratio, although it does make the Raman spectrum more readable.

Matlab was used to derive the optimum width and position of the time gate based on Eq. (1) with different ratios of Raman to fluorescence photons and with a fluorescence time constant of 2 ns (the fluorescence lifetime of sesame seed oil). A specific spectral point has to be chosen for simulating the achievable SNR, because both the fluorescence level and the intensity of the Raman signal can vary as a function of the spectral point. A spectral point of 1442 cm^{-1} was chosen as a reference because one of the highest Raman peak is observed at this point in olive and sesame seed oils [25]. The Matlab simulations were repeated approximately 3,000,000 times to correspond to a measurement result obtained with 3,000,000 laser pulses for each spectral point, as presented below (3,000,000/4000 Hz = > 750 s).

It is obvious that the position of the front edge of the timing window should be set so that most of the Raman photons are collected during the rising part of the laser pulse. A trade-off exists, however, since too early position will increase the dark count noise. The SNRs achieved with 3,000,000 pulses are shown in Fig. 4(c) as a function of the width of the time gate with ratios of Raman to fluorescence photons of 0.3, 0.03 and 0.003 (The number of Raman photons was kept constant and that of fluorescence photons was increased), respectively, when the front edge of the time gate was kept at the same optimal position to keep the dark count noise level minimum based on the simulation. As can be seen in Fig. 4(c), the optimum SNR is achieved with a time gate width which is less than the full width of the laser pulse ($\pm 3\sigma = 1272$ ps) and thus less than the whole Raman distribution. With a lower Raman to fluorescence level ratio the width of the time gate has to be reduced. If the time gate is wider than the optimum, the SNR will gradually decrease, first due to the collecting of fluorescence photons and then mostly due to the dark counts.

Fig. 5 shows the effect of the change of the starting position of the optimal time gate width on the signal-to-noise ratio when the

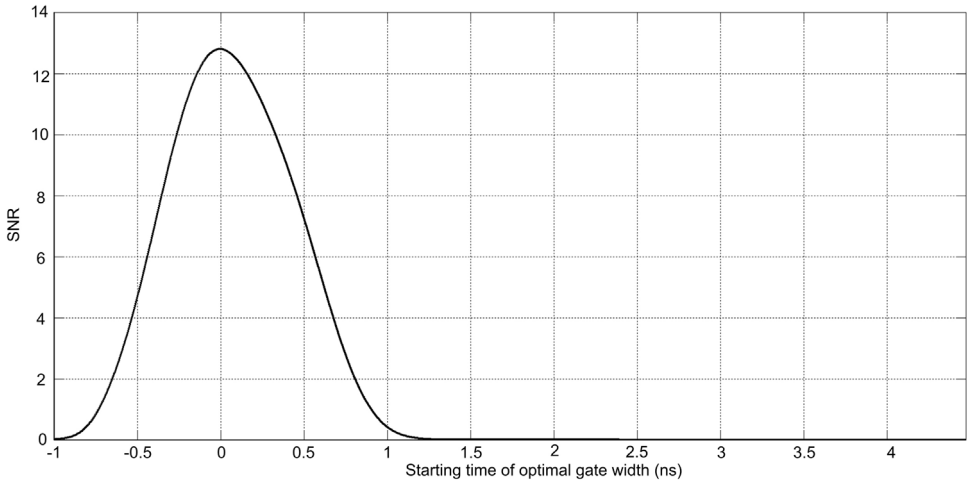

Fig. 5. Signal-to-noise ratios of 3,000,000 pulses as a function of the starting time of the optimal gate width with Raman to fluorescence ratio of 0.003.

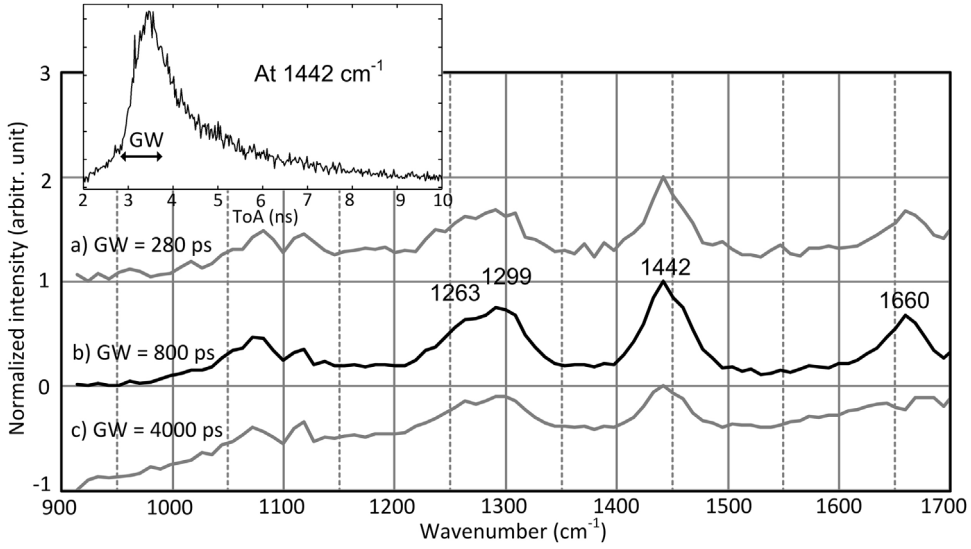

Fig. 6. Raman spectra of olive oil obtained with different time gate widths: a) 280 ps, b) 800 ps and c) 4000 ps.

ratio of Raman to fluorescence photons and the time constant of the fluorescence life time are 0.003 and 2 ns, respectively. As can be seen in Fig. 5, the best possible SNR is achieved by starting the optimal time gate at the zero time position which is approximately the starting point of a laser pulse and thus the Raman signal. If the starting position is generated earlier the signal-to-noise ratio is decreased by mainly the decrease of Raman signal and the increase of the shot noise of dark count photons and if it is generated later the shot noise of fluorescence count photons is increased and the Raman signal is decreased.

4. Measurement results

The effectiveness of the fluorescence rejection was tested by using a 532 nm commercial laser from Teem Photonics having a pulse width of 500 ps and a pulse rate of 4 kHz. A high-precision time interval measurement unit was used to measure the time of arrival of each photon relative to the excitation laser pulse. Histograms of these photons (photon probability distributions) were collected at the each spectral position by changing the position of the SPAD detector with a step motor. Matlab was used to derive Raman spectra from the collected distribution of photons as a function of time with different widths and positions of the time gate. In addition, the residual fluorescence level was approximated by means of another time gate and the residual baseline was subtracted from the result to make the spectrum more readable. The width and position of the time gate were adjusted as guided by the simulations, and the Raman spectra were analyzed to see the effect of the optimization. The advantage of using a step motor and a single SPAD element with a single TAC is that the possible non-homogeneity of SPAD devices and time interval units in an array can be avoided with an expense of the increased measurement time. However, as was mentioned above the aim of this work was to study what kind of performance could be achieved by using an "ideal SPAD array". The olive oil and sesame seed oil used as samples had fluorescence time constants of 2.5 ns and 2 ns, respectively, and Raman to fluorescence photon ratios of ~0.03 and ~0.003, these ratios having been estimated by fitting a Gaussian pulse to various fluorescence and Raman distributions to get similar results to those measured and calculating the ratios of the integrals of the Raman and fluorescence distributions.

The Raman spectra for olive and sesame seed oils have peaks at the same wave numbers, and detailed spectra measured with a Raman spectrometer from Process Instruments based on a 785 nm CW laser have been published previously [25]. The most interesting

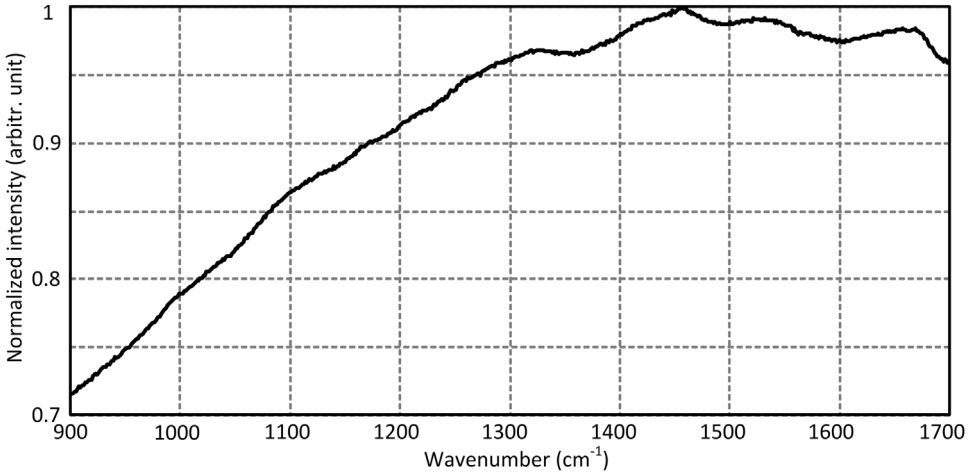

Fig. 7. Raman spectra of sesame seed oil measured by means of a CW laser and CCD array.

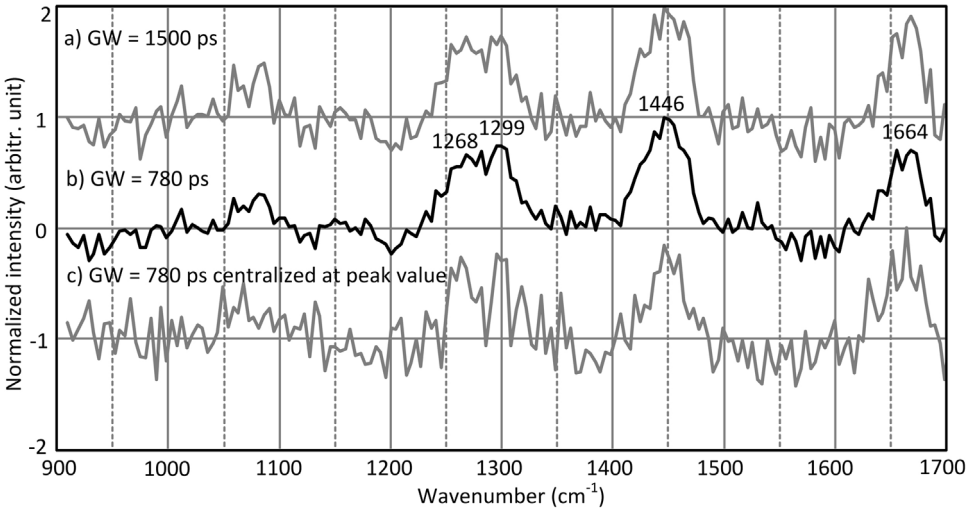

Fig. 8. Raman spectra of sesame seed oil obtained with different widths of the time gate: a) 1500 ps, b) the optimum width, 780 ps, and c) 780 ps centered on the peak value for the time domain distribution.

spectral region for these oils, showing most of the Raman peaks, is between 900 cm^{-1} and 1700 cm^{-1}.

The Raman spectra of the olive and sesame seed oils were derived using approximately 3,000,000 laser pulses at every spectral point to integrate an adequate number of photons, and a single SPAD detector was swept over the wave number range in approximately 9 cm^{-1} steps. The simulations showed that the best possible SNR can be achieved with olive oil using a width of time gate of 820 ps (see Fig. 4(c) ratio 0.03). The measured Raman spectra are shown for gate widths (GW) of 280 ps, 800 ps and 4000 ps, respectively, in Fig. 6(a)–(c). The Raman spectra for the different time gates have simply been shifted in the intensity domain to make the figure clearer. The best possible measured Raman spectrum was achieved with a gate width of 800 ps. It can also be seen from Fig. 6 that other gate widths clearly lead to a deterioration in SNR. As was mentioned above, the Raman spectra were derived from the distribution of the times of arrival of the photons (ToA) with gate widths. One example of such a distribution, measured at 1442 cm^{-1}, is shown in the inset in Fig. 6.

To show the difficulty in deriving a Raman spectrum for sesame seed oil with 532 nm laser excitation, this was also measured using a laboratory Raman spectroscopy device based on a continuous wave (CW) laser and CCD array, yielding the spectrum shown in Fig. 7. As can be seen, no peaks can be distinguished in this Raman spectrum, on account of the one decade higher fluorescence level relative to that for olive oil, resulting in a poorer SNR.

Raman spectra for the sesame seed oil as measured with the time-gated system using a gate width of 1500 ps, the optimally positioned time gate with the optimum width of 780 ps and a gate width of 780 ps centered on the peak value for the combined distribution are shown in Fig. 8(a)–(c), respectively. The measured Raman spectra shown in Fig. 8(a) and (c) have a poorer signal to noise ratio than in the optimal case (shown in Fig. 8(b)), and the signal-to-noise ratio with the same measurement time is almost one decade worse than for olive oil, which can be clearly seen by comparing Figs. 6 and 8 . The spectrum derived using the optimum width and centered on the peak value of the combined distribution also has a lower signal-to-noise ratio, which can be explained by the fact that most of the Raman photons at the beginning of the pulse have been lost, whereas, since the fluorescence level is now ten times larger than that for olive oil, it is more important to start collecting the photons in the early rising part of the laser pulse.

5. Conclusions and discussion

The principle for determining the best possible width and position of a time gate for fluorescence suppression in time-gated Raman spectroscopy has been presented here and the effective-

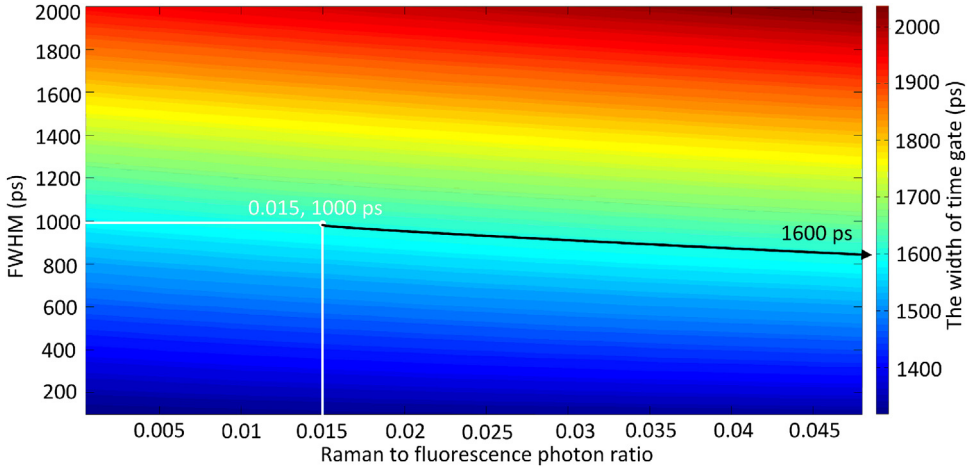

Fig. 9. Map for deriving the prober width of the time gate required to achieve the best possible SNR with a given laser pulse width and Raman to fluorescence intensity ratio.

ness of the techniques has been verified by the Raman spectroscopy measurements. The width and position of the time gate are the most important parameters to consider when attempting to achieve maximum fluorescence suppression, and they will increase in importance whenever the time constant of the fluorescence lifetime approaches the width of the laser pulse and the sample has a high fluorescence background. The starting time, i.e the position of the time gate, should coincide with the early front edge of the laser pulse, but without collecting the dark counts. Our simulations showed that the higher the fluorescence level is in relation to the Raman level, the shorter the width of the time gate has to be in order to achieve the best possible fluorescence rejection and signal-to-noise ratio.

The effectiveness of fluorescence rejection was verified here by measuring the Raman spectra of two challenging samples, olive oil and sesame seed oil, with time constants of their fluorescence lifetime of 2.5 ns and 2 ns, respectively, and ratios of Raman to fluorescence photons of 0.03 and 0.003, respectively. The Raman spectra of both samples could be resolved and uniformity between the simulation and the measurements could be verified.

One practical way of aiming at the best possible signal-to-noise ratio in time-gated Raman spectroscopy is to specify the proper width of the time gate for the selected width of the laser pulse and the ratio of Raman to fluorescence photons. Matlab code was written in order to determine the best possible width of the time gate for a sample having the 2.5 ns time constant for its fluorescence lifetime, i.e. to achieve the best SNR. The simulation result shown in Fig. 8 can be used to specify the proper width of the time gate (colors) for the selected width of the laser pulse (y-axis) and the Raman to fluorescence photon ratio (x-axis) in order to achieve the best possible SNR. For example, if the width of the laser pulse is 1000 ps (FWHM) and the ratio of Raman to fluorescence photons is 0.015, the best signal-to-noise ratio can be achieved with a time gate of width 1600 ps, as shown in Fig. 9 and the front edge of the time gate positioned at the cross-over point of the background and the laser pulse front edge intensity distributions. Fig. 9 also shows the obvious fact that as the Raman to fluorescence photon ratio increases with the laser pulse width, the width of the time gate should also be increased.

Declaration of conflicting interests

The Authors declare that there is no conflict of interest.

Acknowledgements

This work was supported by the Academy of Finland, Centre of Excellence in Laser Scanning Research under Contract 272196, and Contracts 282405 and 292609.

References

[1] E.B. Hanlon, R. Manoharan, T.-W. Koo, K.E. Shafer, J.T. Motz, M. Fitzmaurice, J.R. Kramer, I. Itzkan, R.R. Dasari, M.S. Feld, Prospects for in vivo Raman spectroscopy, Phys. Med. Biol. 45 (2) (2000) R1–R59.
[2] L. Nancy Jestel, Process raman spectroscopy, in: K.A. Bakeev (Ed.), Process Analytical Technology: Spectroscopic Tools and Implementation Strategies for the Chemical and Pharmaceutical Industries, John Wiley and Sons, Chichester, UK, 2010, pp. 195–244, Chapter 7.
[3] O. Khalil, Spectroscopic and clinical aspects of noninvasive glucose measurements, Clin. Chem. 45 (2) (1999) 165–177.
[4] D. Tuschel, Raman spectroscopy of oil shale, Spectrosc. Solutions Mater. Anal. 28 (3) (2013) 920–927.
[5] T. Vankeirsbilck, A. Vercauteren, W. Baeyens, G. Van der Weken, F. Verpoort, G. Vergote, J.P. Remon, Applications of Raman spectroscopy in pharmaceutical analysis, J. Trends Anal. Chem. 21 (12) (2002) 869–877.
[6] Y. Li, J.S. Church, Raman spectroscopy in the analysis of food and pharmaceutical nanomaterials, J. Food Drug Anal. 22 (1) (2014) 29–48.
[7] M.E. Darvin, I. Gersonde, M. Meinke, W. Sterry, J. Lademann, Non-invasive in vivo determination of the carotenoids beta-carotene and lycopene concentrations in the human skin using the Raman spectroscopic method, J. Phys. 38 (15) (2005) 2696–2700.
[8] M. Chena, J. Juuti, C. Hsi, C. Chia, H. Jantunen, Dielectric BaTiO3–BBSZ glass ceramic composition with ultra-low sintering temperature, J. Eur. Ceram. Soc. 35 (1) (2015) 139–144.
[9] P. Matousek, M. Towrie, C. Ma, W.M. Kwok, D. Phillips, W.T. Toner, A.W. Parker, Fluorescence suppression in resonance Raman spectroscopy using a high-performance picosecond Kerr gate, J. Raman Spectrosc. 32 (12) (2001) 983–988.
[10] R.P. Van Duyne, D.L. Jeanmaire, D.F. Shriver, Mode-locked laser raman spectroscopy-A new technique for the rejection of interfering background luminescence signals, Anal. Chem. 46 (2) (1974) 213–222.
[11] N. Everall, R.W. Jackson, J. Howard, K. Hutchinson, Fluorescence rejection in raman spectroscopy using a gated intensified diode array detector, J. Raman Spectrosc. 17 (5) (1986) 415–423.
[12] J. Howard, N.J. Everall, R.W. Jackson, K. Hutchinson, Fluorescence rejection in Raman spectroscopy using a synchronously pumped, cavity-dumped dye laser and gated photon counting, J. Phys. E: Sci. Instrum. 19 (11) (1986) 934–943.
[13] E.V. Efremov, J.B. Buijs, C. Gooijer, F. Ariese, Fluorescence rejection in resonance raman spectroscopy using a picosecond-Gated intensified charge-coupled device camera, Appl. Spectrosc. 61 (6) (2007) 571–578.
[14] D.V. Martyshkin, R.C. Ahuja, A. Kudriavtsev, S.B. Mirov, Effective suppression of fluorescence light in Raman measurements using ultrafast time gated charge coupled device camera, Rev. Sci. Instrum. 3 (2004) 630–635.
[15] A. Rochas, M. Cani, B. Furrer, P.A. Besse, R.S. Popovic, G. Ribordy, N. Gisin, Single photon detector fabricated in a complementary metal-oxide-semiconductor high voltage technology, Rev. Sci. Instrum. 74 (7) (2003) 3263–3270.
[16] I. Nissinen, J. Nissinen, A.-K. Länsman, L. Hallman, A. Kilpelä, J. Kostamovaara, M. Kögler, M. Aikio, J. Tenhunen, A sub-ns time-gated CMOS single photon avalanche diode detector for Raman spectroscopy, in: Paper presented at:

IEEE European Solid-State Device Research Conference (ESSDERC'11), Helsinki, Finland; September 12–16, 2011.
[17] J. Kostamovaara, J. Tenhunen, M. Kögler, I. Nissinen, J. Nissinen, P. Keränen, Fluorescence suppression in Raman spectroscopy using a time-gated CMOS SPAD, Opt. Express 21 (25) (2013) 31632–31645.
[18] I. Nissinen, A.-K. Länsman, J. Nissinen, Jouni Holma, J. Kostamovaara, 2x(4x)128 time-gated CMOS single photon avalanche diode line detector with 100 ps resolution for Raman Spectroscopy, in: Paper presented at: IEEE European Solid-State Circuits Conference (ESSCIRC'13), Bucharest, Romania; September 16–20, 2013.
[19] I. Nissinen, J. Nissinen, P. Keränen, A.-K. Länsman, J. Holma, J. Kostamovaara, A 2x(4)x128 multi-time-gated SPAD line detector for pulsed raman spectroscopy, IEEE J. Sens. 15 (3) (2015) 1358–1365.
[20] I. Nissinen, J. Nissinen, J. Holma, J. Kostamovaara, A 4 (128 SPAD array with a 78-ps 512-channel TDC for time-gated pulsed raman spectroscopy, Springer science and business media, Analog Integr. Circuits Signal Process. 84 (3) (2015) 353–362.
[21] Y. Maruyama, J. Blacksberg, E. Charbon, A 1024x8, 700-ps time-Gated SPAD line sensor for planetary surface exploration with laser raman spectroscopy and LIBS, IEEE J. Solid-St. Circ. 49 (1) (2014) 179–189.
[22] N. Krstajic, R. Walker, J. Levitt, S.P. Poland, D. Li, S. Ameer-Beg, R.K. Henderson, A 256 x 8 SPAD line sensor for time resolved fluorescence and raman sensing, in: Paper Presented At: IEEE European Solid-State Circuits Conference (ESSCIRC'14), Venezia Italy; September 22–26, 2014.
[23] P. Zhou, B.W. Tek, Choosing the Most Suitable Laser Wavelength For Your Raman Application, 2015, http://bwtek.com/wp-content/uploads/2015/07/raman-laser-selection-application-note.pdf (accessed 18.12.15).
[24] D. Mosconi, D. Stoppa, L. Pancheri, L. Gonzo, A. Simoni, CMOS single-Photon avalanche diode array for time-resolved fluorescence detection, in: Paper Presented At: IEEE European Solid-State Circuits Conference (ESSCIRC'06), Montreux Switzerland; September 18–22, 2006.
[25] Process Instruments, Edible Oils: Safflower, Peanut, Olive, Corn, Canola, Vegetable, 2016, http://www.process-instruments-inc.com/pdf/PI_Raman_Cooking_Oils.pdf (accessed 18.12.15).

Biographies

Ilkka Nissinen (M'09) was born in Oulu, Finland, in 1976. He received the M.Sc. Eng., Licentiate of Tech. and Dr. Tech. degrees in electrical engineering from the University of Oulu, Finland, in 2002, 2007 and 2011, respectively. He has been Research Scientist in 2002–2011 and Postdoctoral Researcher since 2011 in Circuits and Systems Research Unit in University of Oulu. His research interests include the design of time interval measurement architectures for the integrated receiver of pulsed time-of-flight laser rangefinders and the development of time-gated single photon avalanche diode arrays for Raman spectroscopy. He has designed or co-designed approximately 10 ASICs during his career and has authored or co-authored 24 scientific papers.

Jan Nissinen was born in Oulu, Finland, in 1976. He received the M.Sc. Eng., Licentiate of Tech. and Dr.Tech. degrees in electrical engineering from the University of Oulu, Finland, in 2002, 2007 and 2011, respectively. He has been Research Scientist in 2002–2011 and Postdoctoral Researcher since 2011 in Circuits and Systems Research Unit in University of Oulu. His research interests include the design of analog and mixed-signal integrated circuits for pulsed time-of-flight laser rangefinders and for pulsed Raman spectroscopy.

Pekka Keränen was born in Tampere, Finland, in 1985. He received the M.Sc. (Tech) and Dr. Tech. degrees in electrical engineering from the University of Oulu, Finland, in 2010 and 2016, respectively. He is currently working as a Postdoctoral Researcher in Circuits and Systems Research Unit in University of Oulu. His main research interest is the design of time interval measurement circuits.

Juha Kostamovaara (M'85, S'13) received the degrees of Dipl. Eng., Lic.Tech. and Dr.Tech in electrical engineering in 1980, 1982 and 1987, respectively, all from the University of Oulu, Finland. He was Acting Associate Professor of electronics in the department of electrical Engineering, University of Oulu, in 1987 −1993, and was nominated Associate Professor from the beginning of 1993. During 1994, he was an Alexander von Humboldt Scholar at the Technical University of Darmstadt, Germany. In 1995 he was invited to become full professor of electronics at the University of Oulu, where he is currently also the Head of the Circuits and Systems Research Unit. In 2007 he was nominated to the Academy professorship position by the Academy of Finland, which position he holds till 2017. His main interests are in the development of high-speed electronic circuits and systems and their applications in electronic and optoelectronic measurements.